frontiers | Frontiers in Marine Science

TYPE Original Research
PUBLISHED 11 October 2024
DOI 10.3389/fmars.2024.1470134

OPEN ACCESS

EDITED BY
Xiaodong Jiang,
Guangdong University of Technology, China

REVIEWED BY
Xi Mei,
Qingdao Institute of Marine Geology (QIMG), China
Jianghu Lan,
Chinese Academy of Sciences (CAS), China

*CORRESPONDENCE
Zhongshan Shen
zsshen@mail.iggcas.ac.cn
Haifeng Wang
wanghaifeng112@163.com

RECEIVED 25 July 2024
ACCEPTED 18 September 2024
PUBLISHED 11 October 2024

CITATION
Shen Z, Chen Y, Mikhailik P, Cai Y, Wang H and Yi L (2024) Early diagenesis, sedimentary dynamics and metal enrichment reveal deep-sea ventilation in Magellan Seamounts during the middle Pleistocene.
Front. Mar. Sci. 11:1470134.
doi: 10.3389/fmars.2024.1470134

Early diagenesis, sedimentary dynamics and metal enrichment reveal deep-sea ventilation in Magellan Seamounts during the middle Pleistocene

Zhongshan Shen[1]*, Yanping Chen[2], Pavel Mikhailik[3], Yun Cai[4], Haifeng Wang[5,6]* and Liang Yi[4]

[1]State Key Laboratory of Lithospheric and Environmental Coevolution, Institute of Geology and Geophysics, Chinese Academy of Sciences, Beijing, China, [2]Zhejiang Academy of Marine Sciences, Second Institute of Oceanography, Ministry of Natural Resources, Hangzhou, China, [3]Laboratory of Regional Geology and Tectonic, Far East Geological Institute, Far East Branch of Russian Academy of Sciences, Vladivostok, Russia, [4]State Key Laboratory of Marine Geology, Tongji University, Shanghai, China, [5]Key Laboratory of Marine Mineral Resources, Ministry of Natural Resources, Guangzhou Marine Geological Survey, China Geological Survey, Guangzhou, China, [6]Southern Marine Science and Engineering Guangdong Laboratory (Guangzhou), Guangzhou, China

Seamounts are ubiquitous topographic units in the global oceans, and the Caiwei Guyot in the Magellan Seamounts of the western Pacific is a prime example. In this study, we analyzed a well-dated sediment core using magnetic properties, sediment grain size, and metal enrichment to uncover regional ventilation history during the middle Pleistocene and explore potential linkages to global climate changes. Our principal findings are as follows: (1) The median grain size is 3.3 ± 0.2 μm, and clay and silt particles exhibit minimal variation, with average values of 52.8 ± 1.8% and 38.2 ± 1.6%, respectively, indicating a low-dynamic process; (2) Three grain-size components are identified, characterized by modal patterns of ~3 μm (major one), ~40 μm, and 400–500 μm, respectively; (3) Magnetic coercivity of the deep-sea sediments can be classified into three subgroups, and their coercivity values are 6.1 ± 0.5 mT, 25.7 ± 1.0 mT, and 65.2 ± 2.1 mT. Based on these results, we propose a close linkage between magnetic coercivity and metal enrichment, correlating with changes in deep-sea circulation intensity. Conversely, sediment grain-size changes seem to be more strongly influenced by eolian inputs. Consequently, we suggest that regional ventilation has weakened since ~430 ka, likely linked to a reduction in Antarctic bottom water formation.

KEYWORDS

abyssal ventilation, early diagenesis, magnetic properties, Caiwei (Pako) Guyot, middle Pleistocene, western Pacific

1 Introduction

More than 50,000 seamounts have been identified in the Pacific Ocean, and the Magellan Seamounts, formed by hotspot activity during 120–90 Ma (Wessel, 1997; Wessel and Lyons, 1997; Stepashko, 2008), include the Caiwei, the Vlinder, and the Loah, and are distributed in a northwestward chain (Figure 1). Among them, the Caiwei Guyot, a well-studied deep-sea flat-topped seamount, has water depths of ~1 500–1 600 m at its summit and ~5 500 m at its base. The Caiwei Guyot is situated within the main flow path of the Antarctic bottom water (AABW) and Lower Circumpolar Deep Water (LCDW) as they move toward the North Pacific, and the former, AABW, is considered a potential intermediary in the influence of the Antarctic on global climate change (Talley, 2008; Kawabe and Fujio, 2010). It covers >70% of the ocean-bottom region and represents 30%–40% of the total global water mass (Johnson, 2008). With its high level of dissolved oxygen, the AABW significantly contributes to abyssal ventilation and redox conditions (Gordon, 2001). Furthermore, an anti-cyclonic eddy has been identified over the guyot (Guo et al., 2020), contributing to similar hydrochemical properties around the seamount, such as salinity, pH value, and nitrate, likely influenced by this anti-cyclonic phenomenon (Liu et al., 2019). Previous studies focusing on mineral resources and megafaunal communities (Wang et al., 2016b; Xu et al., 2016) and microorganisms (Liu et al., 2019; Sun et al., 2020; Yang et al., 2020) have proposed that cobalt-rich crusts, carbonate rocks, and calcareous pelagic deposits are the main dominant sediments on the guyot (He et al., 2001; Wei et al., 2017; Zhao et al., 2020). This unique seafloor topography, which rises from the open ocean, also enhances nutrient transport, supporting the local ecosystem (Wang et al., 2024).

Despite these insights, our understanding of the complex deep-sea environment remains incomplete. Cross-validation of different proxies for paleoenvironmental reconstruction has been limited. For example, dissolute-oxygen reconstruction, a key issue in deep-sea environmental inferences, has not been thoroughly examined. In this study, we utilize three widely used proxies, namely early diagenesis, metal enrichment, and sediment grain size, to infer the paleoenvironmental conditions of the Caiwei Guyot, situated in an area strongly influenced by AABW/LCDW circulation (Figure 1). By integrating magnetostratigraphy and authigenic beryllium isotopes ($^{10}Be/^{9}Be$), we have constructed a reliable age-depth model for the studied core. Using this geochronological framework, we discuss the magnetic and grain-size properties in conjunction with metal enrichment in abyssal sediments in this unique region since ~440 ka.

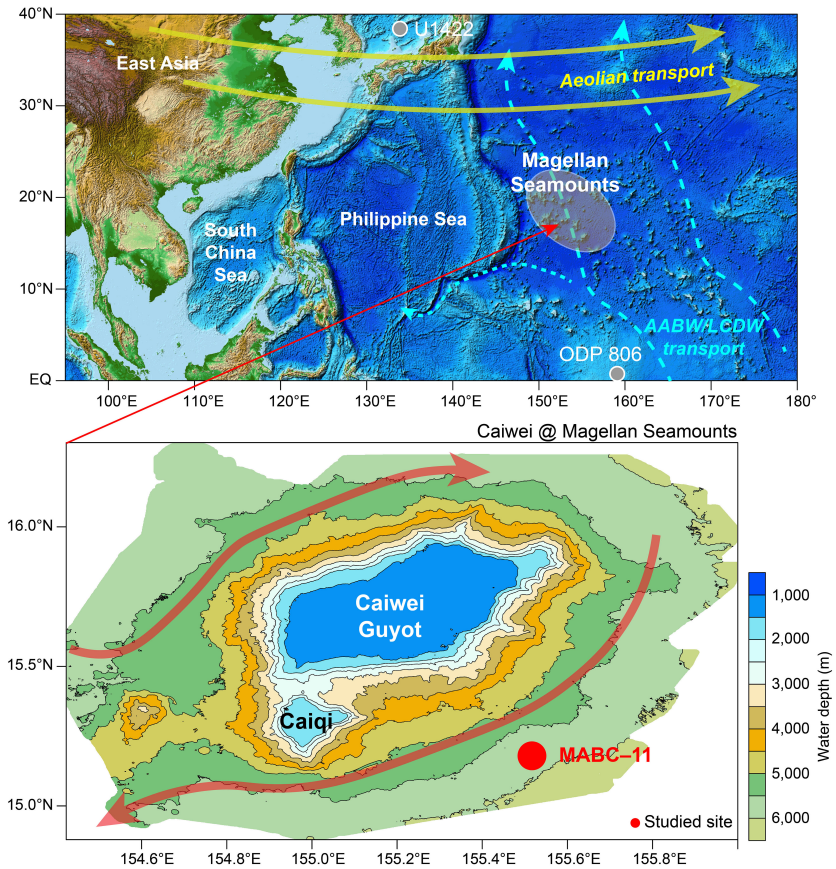

FIGURE 1
Schematic map showing the study site (MABC–11) and oceanographic setting. The flows were modified from previous works (Guo et al., 2020; Kawabe and Fujio, 2010; Zhai and Gu, 2020). AABW, Antarctic bottom water; LCDW, Lower Circumpolar Deep Water. U1422 and ODP 806 are the referenced sites mentioned in the main text.

2 Methods

2.1 The studied core

Core MABC–11 (155.53° E, 15.22° N, 5,840 m water depth) was retrieved from the eastern base of the Caiwei Guyot (Figure 1) using a box corer aboard R/V *Haiyang Liu Hao* in July 2012, with a core length of 59 cm.

The age model of core MABC–11 was developed using magnetostratigraphy and by tuning changes in element Ca intensity (from XRF scanning) with the deep-sea benthic $\delta^{18}O$ stack LR04 (Lisiecki and Raymo, 2005), which reflects global ice volume changes. The resulting average sedimentation rate is 0.73 mm/kyr (Yi et al., 2021a). To further refine the chronology, this age-depth model was adjusted based on $^{10}Be/^{9}Be$ data to integrate deep-sea paleoenvironmental records from the Mariana Trench and Magellan Seamounts (Yi, 2023). For this study, the core was sampled for the depth interval of 7.0–49.5 cm at 5 mm resolution, and 86 subsamples in total were obtained for magnetic and grain-size analyses between 221 and 904 ka (Figure 2).

2.2 Magnetic measurement

Hysteresis loops were conducted on all 86 samples using a Princeton Measurements Inc. MicroMag 3900 Vibrating Sample Magnetometer (VSM). A peak field of 0.3 T was set for hysteresis loops, and saturation magnetization (Ms), saturation remanence (Mrs), coercive force (Bc), and the coercivity of the remanence (Bcr) were determined from the hysteresis loops, after calibration using the data from between 0.25 and 0.30 T. All magnetic measurements were conducted at the Paleomagnetism and Geochronology Lab (PGL), Institute of Geology and Geophysics, Chinese Academy of Sciences.

The mathematical unmixing of hysteresis loops can provide detailed information about different coercivity spectra (Jackson et al., 1990). The polymodal distribution for unmixing in this study is expressed as follows:

$$F = p_1 f_1 + \ldots + p_i f_i;\ \sum_1^n p_i = 1 \tag{1}$$

where f_i represents the function for component i where $i = 1$ to n components, and p_i is the percentage contribution of the components. A series of target functions has been proposed for unmixing (Heslop, 2015); here, we used the normal function to identify the potential end members of magnetic minerals in the sediments (Heslop, 2015; Heslop and Roberts., 2012). The normal function has the following form:

$$F = p_1 \frac{1}{\sqrt{2\pi}\alpha_1} e^{-\left[\frac{(x-\beta_1)^2}{2\alpha_1^2}\right]} + p_2 \frac{1}{\sqrt{2\pi}\alpha_2} e^{-\left[\frac{(x-\beta_2)^2}{2\alpha_2^2}\right]} + p_3 \frac{1}{\sqrt{2\pi}\alpha_3} e^{-\left[\frac{(x-\beta_3)^2}{2\alpha_3^2}\right]} \tag{2}$$

Here, x is the independent variable and represents the magnetic field, and the dependent variables are the second derivatives of the hysteresis loop data, which were first standardized to the interval of

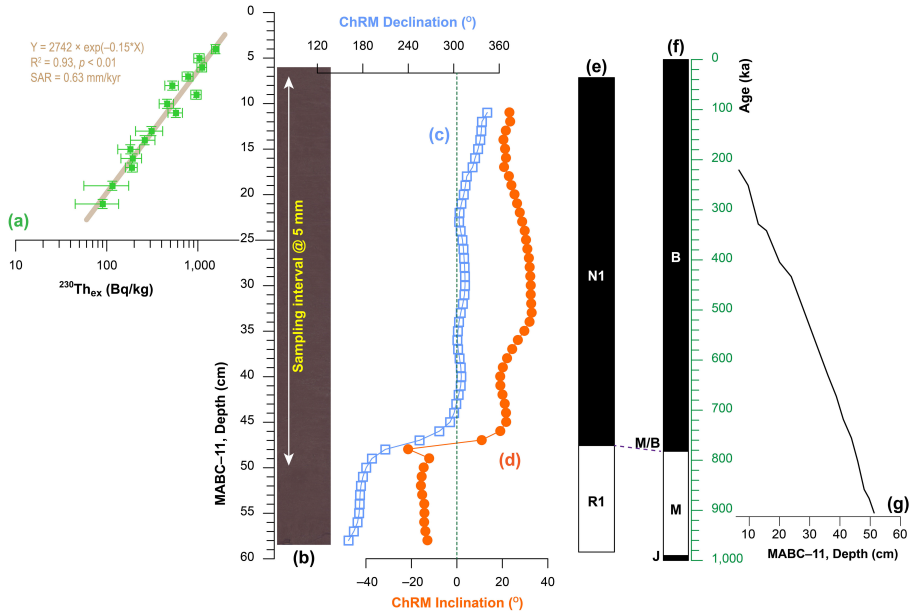

FIGURE 2
Core MABC–11 with the age-depth model during the middle Pleistocene. **(A)** The excess ^{230}Th data and the estimated SAR for the upper part (Yang et al., 2020); **(B)** photo of the core; **(C–E)** ChRM declination and inclination, with the polarity of core MABC–11 (Yi et al., 2021a); **(F)** The geological polarity timescale (GPTS) (Hilgen et al., 2012). B, Brunhes chron; M, Matuyama chron; J, Jaramillo subchron; M/B, the Matuyama/Brunhes boundary. **(G)** The modified age-depth model of core MABC–11 (Yi, 2023).

[0, 4]. The coefficient p represents the relative ratio between three components (namely Cnt1–3), α determines the distribution shape (namely Shp1–3), and β controls the position of the central tendency of the curve, herein, the magnetic coercivity (namely Coe1–3).

2.3 Grain-size measurement

Grain-size samples were placed in an ultrasonic vibrator with sodium hexametaphosphate [$(NaPO_3)_6$] for several minutes to facilitate dispersion and were measured using a Malvern Mastersizer 2000 grain size analyzer in the Key Laboratory of Engineering Oceanography, Second Institute of Oceanography, Ministry of Natural Resources of China.

Fifty grain-size classes between 0.1 and 2000 μm were exported for further analysis. The grain-size distributions were then analyzed by using mathematical methods, including the varimax-rotated principal component analysis (VPCA), environmentally sensitive components, and lognormal-based unmixing (modified from Equation 2), and the common signal of deep-sea dynamics was extracted by a PCA on the studies cores for paleoenvironmental inferences, following the procedures reported in previous studies (e.g., Chen et al., 2021; Paterson and Heslop, 2015; Yi et al., 2022).

3 Results

3.1 Grain-size properties

The median grain-size value (M) of the sediment is 3.3 ± 0.2 μm, indicating a low-dynamic sedimentary environment that remained relatively stable throughout the middle Pleistocene (Figure 3B). The proportions of clay (< 4 μm) and silt (4~63 μm) particles display minimal variation, with average values of 52.8 ± 1.8%, and 38.2 ± 1.6%, respectively, while sand particles (> 63 μm) exhibit greater variability, averaging 9.0 ± 2.6%. Notably, coarse components, likely authigenic micro-nodules (>200 μm), are present in several samples, consistent with slow sediment accumulation in marine environments (Wang et al., 2016a), and are observed in surrounding regions (Yi et al., 2022, 2020).

The grain-size distributions are multi-modal, with modal sizes of approximately 3 μm (dominant), ~40 μm, and 400-500 μm

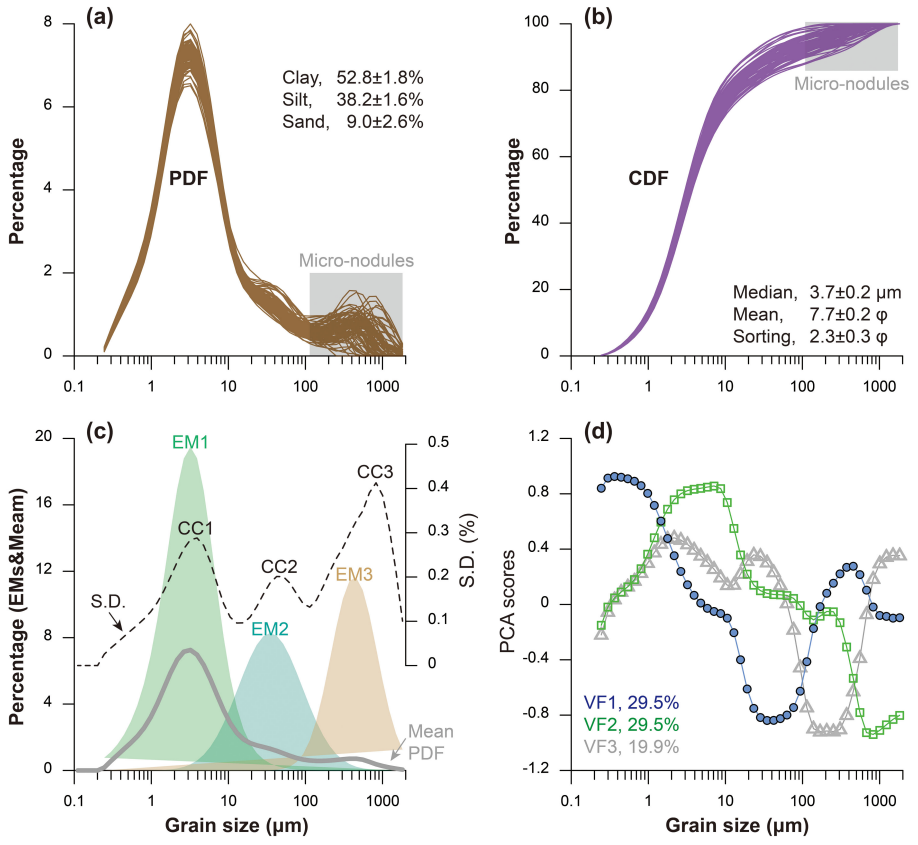

FIGURE 3
Sediment grain-size characteristics of core MABC–11. **(A, B)** Grain-size distribution; PDF, probability density function, CDF, cumulative density function. **(C)** Mathematical unmixing; EMs are the main grain-size components; CCs are the components of the grain-size sensitive fraction; Mean PDF, the average grain-size curve of all samples; S.D., the standard deviation for all samples. **(D)** Principal component analysis (PCA) results; VFs are the leading principal components.

10.3389/fmars.2024.1470134

TABLE 1 Results of the principal component analysis of the sediment grain size of core MABC-11.

Component	Initial Eigenvalues/Extraction Sums of Squared Loadings		
	Total	% of variance	Cumulative %
VF1	13.58	29.5	29.5
VF2	13.56	29.5	59.0
VF3	9.15	19.9	78.9

(Figure 3). Only minor differences were found in the grain-size distributions across different samples, suggesting a stable sedimentary environment during the examined interval. Following the method of Boulay et al. (2003), which has proven effective for identifying sedimentary processes and dynamics (e.g., Hu et al., 2021; Sun et al., 2003), we identified three environmentally sensitive grain-size components (CC1-CC3), with modal sizes of 2.6-4.8 μm, 42.2-51.5 μm, and 676-1000 μm, respectively (Figure 3C).

Polymodal grain-size spectra can be mathematically partitioned (Ashley, 1978), enabling the separation of orthogonal modes (independent grain-size components/factors) to identify potential changes in input functions and/or sedimentary dynamics (e.g., Chen et al., 2020, 2021; Yi et al., 2012b). Using a three-component lognormal function following the method of Paterson and Heslop (2015), which is similar to Equation 2, we obtained three components, EM1, EM2, and EM3 (Figure 3C), with modal sizes of 3.2 μm, 34.6 μm, and 455 μm, respectively. VPCA can also be used to identify the processes controlling sediment grain-size changes and to extract paleoenvironmental signals (e.g., Hu et al., 2021; Yi et al., 2012a). Similarly, the results of VPCA also identify three characteristic components, VF1-VF3 (Figure 3D), accounting for 78.9% in total (Table 1).

Combining all the grain size results, including the environmentally sensitive components (CC1-CC3), lognormal-based unmixing (EM1-EM3), and VPCA results (VF1-VF3), there are three grain-size components similarly identified with a major group (modal sizes at ~3-4 μm), suggesting a single dominant factor controlling sedimentary dynamics in the study area during the depositional interval.

3.2 Magnetic coercivity from unmixing loop curves

Previous studies on magnetic minerals in the Caiwei Guyot sediments, including hysteresis loop, IRM acquisition, and first-order reversal curve analyses, demonstrate that low-coercivity magnetite is the dominant magnetic mineral, with fine grains (Lin et al., 2019; Yi et al., 2021b). Similar mineral properties have been documented at IODP Site U1337 in the eastern Pacific (Yamazaki, 2012), and core XTGC1311 from the middle Pacific (Li et al., 2020).

Hysteresis loop analysis of all 86 samples reveals that the magnetic loops are closed below 200 mT (Figure 4A), indicating a dominance of low-coercivity magnetic minerals. The coercivity values (Bc and Bcr) average 11.4 ± 0.3 mT and 31.5 ± (< 0.05) mT, respectively. On the Day plot (Day et al., 1977), the samples plot within the PSD range, close to the SD field (Figure 4B). Despite minimal variation on the Day plot, a higher Bcr/Bc and Mrs/Ms ratio prior to ~500 ka suggests slightly coarser magnetic grains (Roberts et al., 2018). A three-component lognormal function was applied to mathematically unmix the hysteresis loops (Heslop, 2015; Heslop and Roberts., 2012), yielding coercivity components (Coe1-Coe3) of 6.1 ± 0.5 mT, 25.7 ± 1.0 mT, and 65.2 ± 2.1 mT, respectively (Figure 5). A similar analysis was also applied to unmix the IRM acquisition curves (Maxbauer et al., 2016), and a comparison between hysteresis loop-based and IRM acquisition-based results shows no significant differences (Yi et al., 2021b), and thus is not plotted here.

In a log-normal based unmixing (Equation 2), we employed three parameters to describe a subpopulation of magnetic coercivity, α, β, and p, in which α determines the shape of the distribution (Shp1–Shp3), representing each magnetic type/source/mineral, β controls the position of the central tendency of the curve (Coe1–Coe3), herein representing magnetic coercivity or degree of early diagenesis for each magnetic group, and p indicates the relative

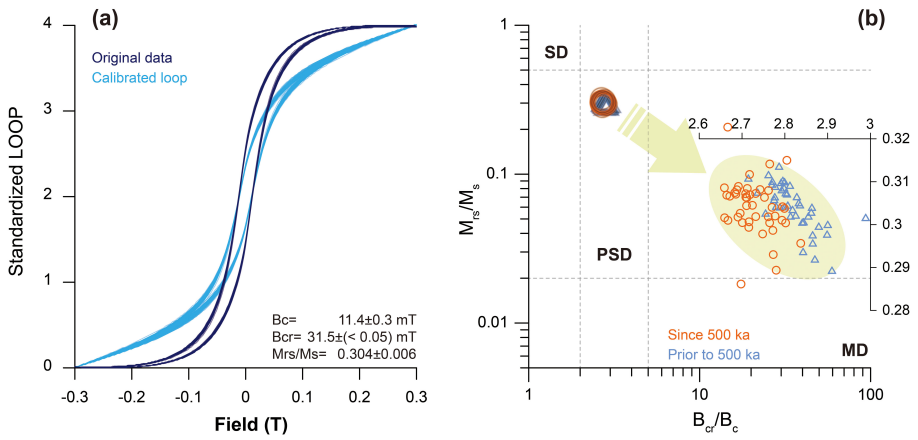

FIGURE 4
Hysteresis loops of all samples in original (blue lines) and calibrated (black lines) forms **(A)**, and Day plot **(B)** of all samples. SD, single domain; PSD, pseudo–single domain; MD, multiple domain.

percentage of each component in a population (Cnt1–Cnt3), representing the ratio of each magnetic group against the total.

Since the source of magnetic minerals in the western Pacific was relatively stable (Chen et al., 2023), the coercivity spectrum can be expressed by these three parameters, and plotting these three parameters together can provide useful information to assess how magnetic minerals changed after deposited (Figure 5). As shown, the major component is Coe2, accounting for about 47%–50% of total magnetic grains in the sediment. Moreover, there is no distinct difference between the pattern of α-β for components Coe2 and Coe3, indicating that these two magnetic groups were linked to a similar source and/or experience similar post-deposition changes (early diagenesis). However, for component Coe1, a more complex relationship between the three magnetic parameters is observed (Figure 5A). Considering all of these observations, together with the close relationship between the derived magnetic components (Figure 5D), component Coe2 was employed for later analysis.

4 Discussion

4.1 Comparison between three ventilation proxies

There are several proxies for studying deep-sea ventilation, including the enrichment of oxygen-sensitive metals (such as Mn, Zn, Ni, and V), sediment grain size, and magnetic coercivity. For instance, element Mn migrates from reducing to oxidizing environments, making it highly sensitive to sedimentary redox changes (Costa et al., 2018; Löwemark et al., 2014; Slemons et al., 2012; Yi et al., 2023). Conversely, sediment grain size reflects the intensity of bottom-water flows, where coarser particles suggest higher sedimentary dynamics and intensified bottom waters, as reported in previous studies (e.g., Hall et al., 2001; Yi et al., 2022). Magnetic properties of deep-sea sediments also offer potential insights into deep-water redox conditions (e.g., Chang et al., 2016; Kissel et al., 2020; Kruiver and Passier, 2001) due to conversions between Fe^{2+} and Fe^{3+} in crystal lattices in the context of oxygen-rich bottom water. However, the exact influence of early diagenesis expressed by changes in magnetic mineral properties may vary between sites because investigations with different oxidation states show that PSD magnetite could be significantly negatively correlated to partial oxidation in a shell-only model, or positively correlated in cases of changing magnetite sizes (Ge et al., 2014; Chen et al., 2023). Hence, considering that the Mn record of core MABC–11 has been cross-validated in previous studies (Yi et al., 2021a; Yi, 2023), we take the Mn record as a reference and compare all of the three proxies to reveal the potential linkages between them (Figures 6–8).

The Mn-enriched sedimentary record from core MABC–11 shows a significant increase in Mn concentration, concurrent with a decrease in sediment median grain size (Figure 6). This observation is contrary to the typical linkage between sediment grain size and bottom-water intensity reported in previous studies (e.g., Hall et al.,

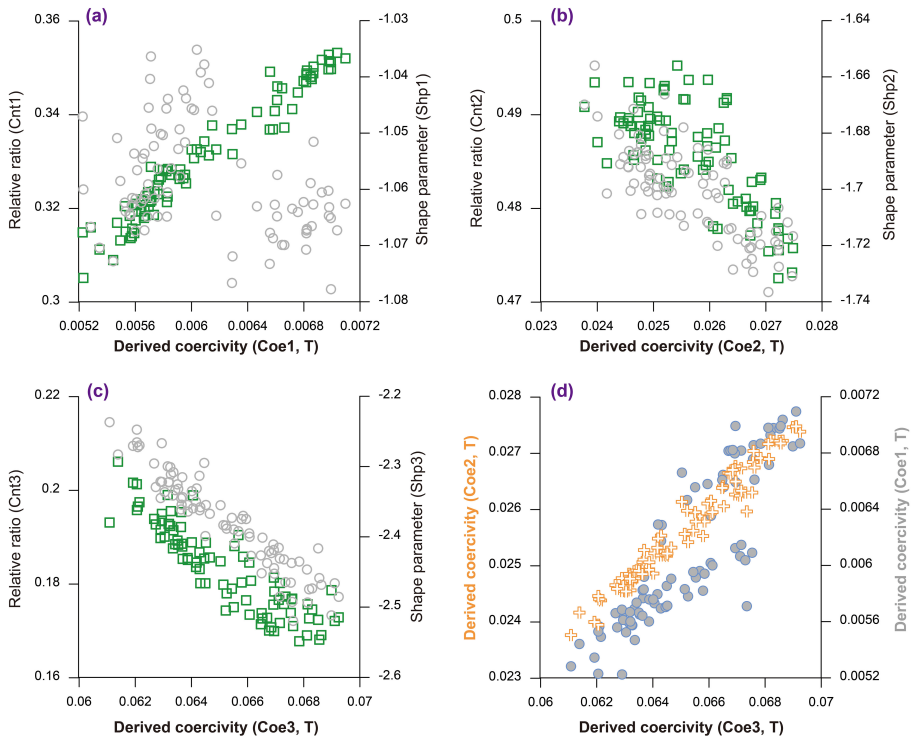

FIGURE 5
Unmixed parameters from hysteresis loops of all samples. **(A–C)** Three magnetic components, **(D)** Coercivity comparison. The relative ratios between the three components were labeled as Cnt1–3, the distribution shapes were labeled as Shp1–3, and the positions of the central tendency of the curve indicating the magnetic coercivity were labeled as Coe1–3.

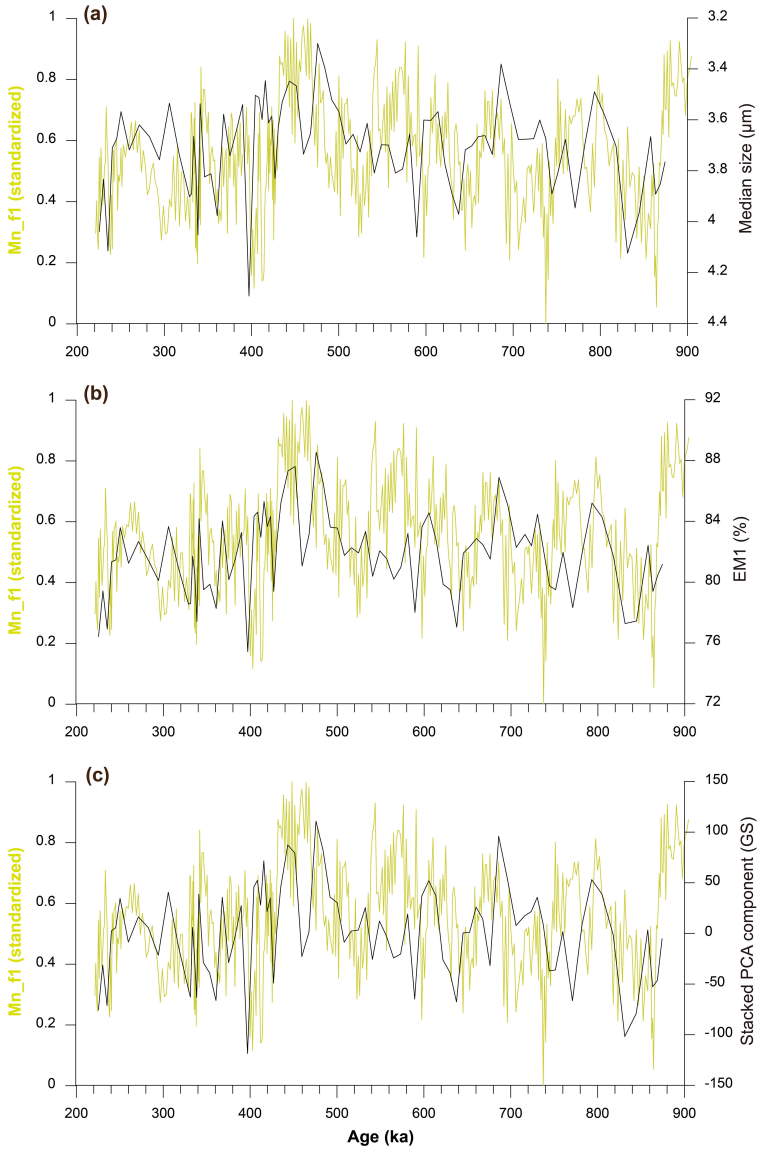

FIGURE 6
Comparison between the sedimentary Mn (Mn_f1) and grain-size variation of core MABC−11 in the middle Pleistocene. **(A)** Median size, **(B)** EM1, **(C)** PCA scores. GS is the integrated record of the three PCA components, namely GS=29.5×VF1 + 29.5×VF2 + 19.9×VF3 (Table 1). Mn−f1 was derived from element ratios of Mn/Cl, Mn/K, Mn/Ca, Mn/Ti, and Mn/Fe, representing the common signal of three cores (MABC-11, J11b, and A25) linked to the regional bottom-water changes (Yi, 2023).

2001; Lamy et al., 2024), suggesting that other processes beyond bottom-water intensity are involved.

Aeolian inputs, which are increasingly recognized as important contributors to deep-sea sedimentation in the western Pacific, may have played a major role, particularly since the middle Pleistocene (Yi et al., 2020, 2022; Yao et al., 2021). The grain-size variation observed in core MABC−11 is generally consistent with records of drying processes in the Asian interior (Figure 7A), inferred from the $\delta^{13}C$ record of the Taklimakan Desert (Liu et al., 2020), and eolian transport to the Japan Sea (Figure 7B), implied from the K content of IODP Site U1422 (Zhang et al., 2018). Fine grains in deep-sea sediments in the North Pacific were mainly carried by the westerlies and/or winter monsoons from the Asian interior (e.g., Rea, 1994; Jiang et al., 2019; Xu et al., 2015), inferring that aridification in inner Asia would result in more eolian particles in deep-sea sediment and a decrease in sediment grain size.

Moreover, seamounts, such as Caiwei Guyot, exert unique influences on regional circulation, vertical mixing, and sediment transport (Bograd et al., 1997; Chen et al., 2015; Yang et al., 2017; Zhang and Boyer, 1993, 1991). For example, a series of complex responses, such as the anticyclonic cap (Lavelle and Mohn, 2010), are generated to modulate regional circulation when currents flow across a seamount (Perfect et al., 2018; Robertson et al., 2017). By studying sediment grain-size properties in the central Philippine Sea, the agreement between deep-sea sedimentary dynamics and ENSO-like changes was highlighted in the Quaternary, suggesting the long-term influence of upwelling and unique submarine topography (Yi et al., 2022). Similarly, in a 3-year monitoring study, a deep anticyclonic cap over the studied guyot was proposed (Guo

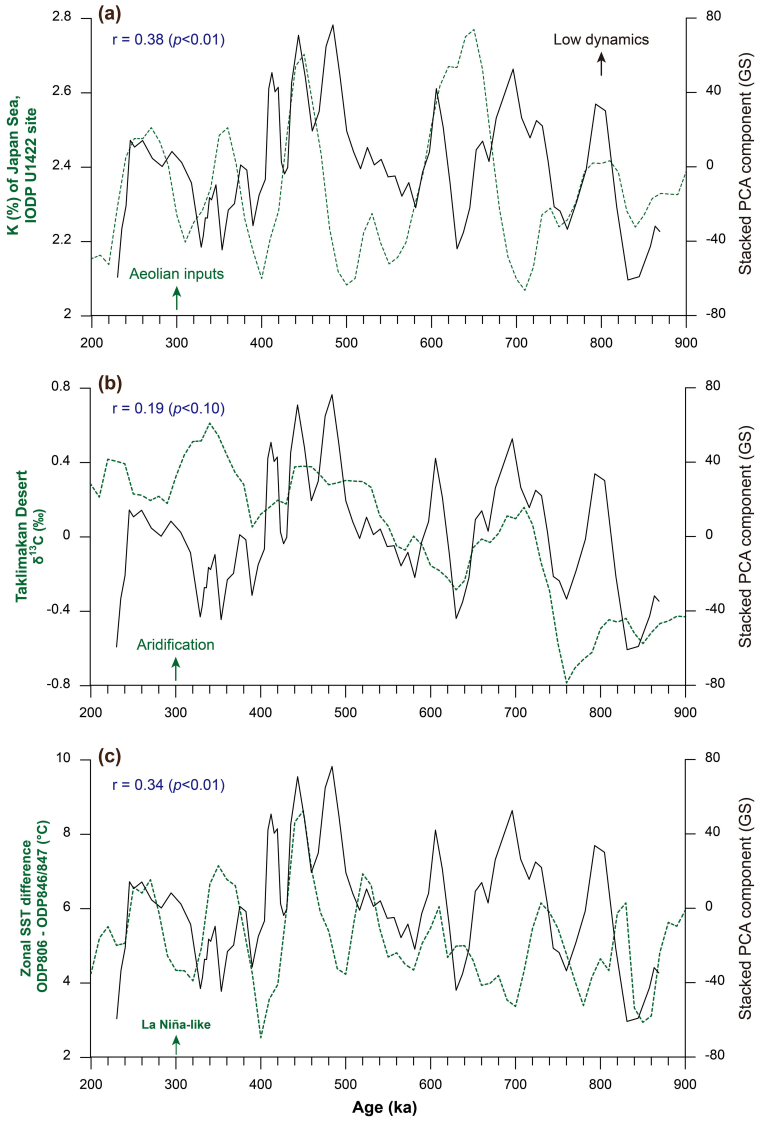

FIGURE 7
Comparison between the grain-size variation of core MABC−11 (GS, 3-point moving average) and various paleoenvironmental proxies in the middle Pleistocene. **(A)** the K content of IODP Site U1422 in the Japan Sea (Zhang et al., 2018), **(B)** the $\delta^{13}C$ record of a sediment core from Lop Nur in the Taklimakan Desert (Liu et al., 2020), and **(C)** the zonal SST difference between ODP Sites 806 and 846/847 (Fedorov et al., 2015). The correlation coefficients in **(A–C)** are r = 0.38 (p<0.01), 0.15 (p<0.10), and 0.34 (p<0.01), respectively. See the aforementioned notes.

et al., 2020), and this topography-induced downwelling could have imparted evident precessional signals into the sedimentary Mn of core MABC–11 (Yi et al., 2021a). Based on this vertical connection in the study area, the downwelling processes could result in more eolian particles being deposited into deep-sea sediments, agreeing with the relationships between the Mn and grain-size records observed in core MABC–11 (Figure 6) and between the zonal SST difference (ENSO-like changes) and MABC–11 grain-size record (Figure 7C). Therefore, it is inferred that eolian inputs may be the dominant factor controlling the sedimentary dynamics in the Caiwei Guyot during the middle Pleistocene.

For magnetic proxies, it is observed that as the Mn contents increase in core MABC–11, the coercivity values of the magnetic components decrease (Figure 8). This inverse relationship between magnetic coercivity and Mn record suggests that redox conditions influenced the preservation and alternations of magnetic minerals in deep-sea sediments.

The relationship between magnetic coercivity and deep-sea redox conditions has been demonstrated using surficial sediments in the Philippine Sea and its surrounding area, and the results show that for PSD magnetite, in higher deep-water oxidation conditions, early diagenesis could result in a lower coercivity of the sediments, and vice versa (Chen et al., 2023). In such a case, prolonged exposure of magnetic minerals to oxygen-rich bottom waters leads to the maghemitization of magnetite grains, which reduces their coercivity. This observation is consistent with experimental studies, in which the partial oxidation of PSD magnetite grains in a core-shell model can decrease the effective diameter of magnetite grains, resulting in a lower coercivity value (Ge et al., 2014; Özdemir and Dunlop, 2010). However, offsets between the Coe2 and Mn_f1 records are also evident (Figure 8),

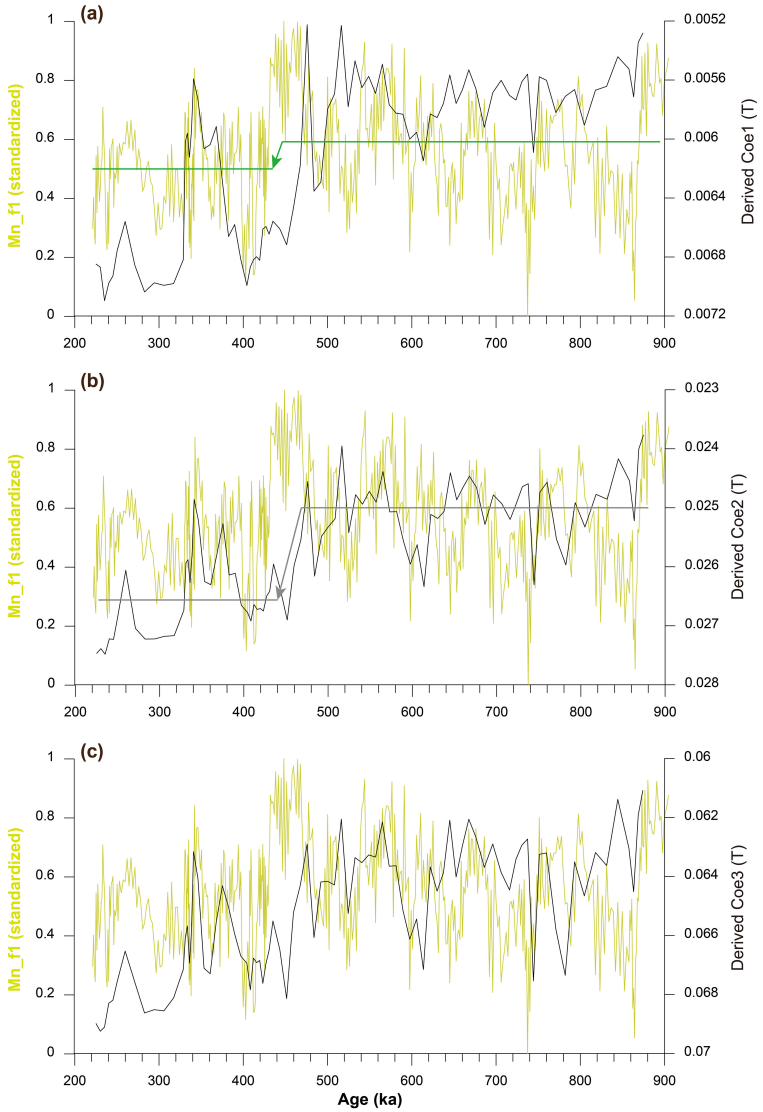

FIGURE 8
Comparison between the sedimentary Mn and magnetic coercivities of core MABC−11 in the middle Pleistocene. **(A–C)** Three coercivity components compared with Mn changes. The arrows in **(A, B)** indicate a significant change across the MBE. The average values of the Coe2 record prior to and post-MBE are 25.0 ± 0.6 mT and 26.5 ± 0.7 mT, respectively. The average values of the Mn_f1 record prior to and post-MBE are 0.50 ± 0.16 and 0.59 ± 0.18, respectively. See the aforementioned notes.

which can be attributed to that the relationship between magnetic coercivity and redox conditions may be influenced by other factors, such as the magnetic grain size, mineralogy, and concentration (Chen et al., 2023). Hence, the observed relationship between magnetic coercivity and sedimentary Mn likely reflects changes in bottom-water oxygenation in the study area and can serve as a proxy for deep-sea ventilation (Figure 9).

4.2 Ventilation history of the Magellan Seamounts

Integrated evidence suggests that significant changes in regional ventilation occurred in the Magellan Seamounts during the middle Pleistocene (Figure 9). To exclude potential dominant influences from marine productivity on abyssal redox conditions, a comparison was conducted between the sedimentary Mn of core MABC–11 and the planktonic $\delta^{13}C$ record from ODP Site 806 (Schmidt et al., 1993). No significant correlation was observed between these records (Yi, 2023), suggesting that ventilation changes were the primary driver of redox conditions rather than changes in productivity in the study area. These proxies reveal a weak but observable in-phase relationship between abyssal ventilation and the LR04 record (Lisiecki and Raymo, 2005), likely indicating intensified deep-sea ventilation during interglacial intervals. This finding aligns with other records from the North Pacific (Jacobel et al., 2017), and further highlights the complex relationship between global glacial-interglacial cycles and deep-sea circulation.

Moreover, glacial intensification of abyssal ventilation is clearly evident during MIS 12, consistent with similar findings in the eastern

10.3389/fmars.2024.1470134

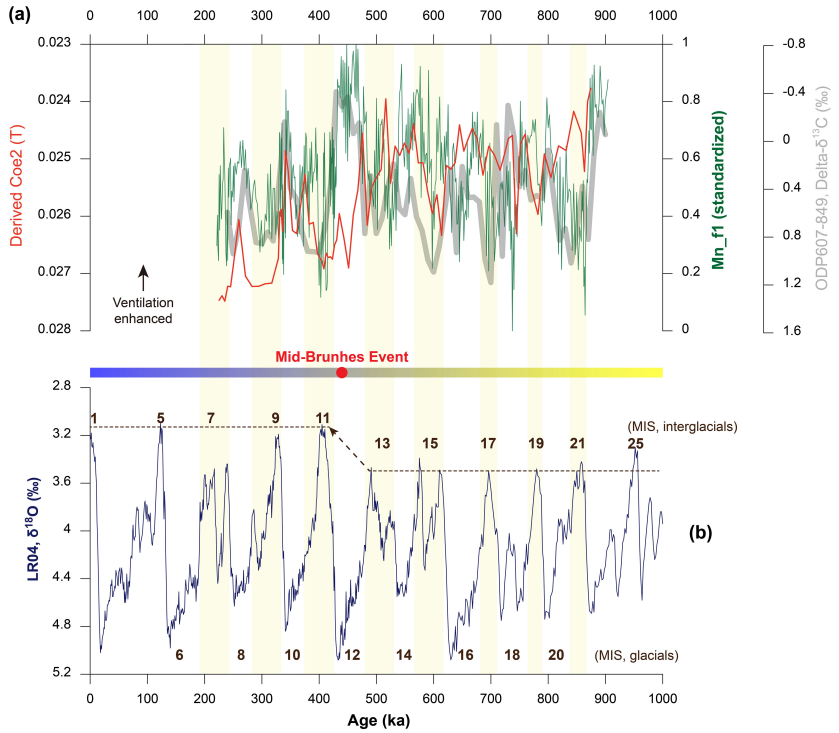

FIGURE 9
Ventilation history of the study region (Caiwei Guyot) in the middle Pleistocene. **(A)** Two proxies of regional ventilation derived from the sediments of core MABC−11 vs. the $\delta^{13}C$ gradient between ODP sites 607 and 849 (Hodell and Venz-Curtis, 2006). **(B)** The benthic $\delta^{18}O$ stack LR04 (Lisiecki and Raymo, 2005). MIS, marine isotope stages, which are labeled as numbers 1–25 at the top. See the aforementioned notes.

Pacific (Yi et al., 2023) and the southwestern Pacific (Hall et al., 2001). The diversity of abyssal ventilation in the study area between glacial and interglacial alternations may be attributed to the redistribution of bottom/deep water masses within the deep Pacific (Yi, 2023), which is worthy of further investigation in the future.

Furthermore, a long-term trend of decreasing abyssal ventilation since ~430 ka (Figure 8) coincides with the Mid-Brunhes Event (MBE), a period characterized by enlarged amplitudes in the glacial-interglacial cycles (Figure 9B). Whether the MBE represents multiple equilibria in the climate system (Jansen et al., 1986; Paillard, 1998), or a transition between two distinct climate states singly responding to astronomical forcing (Tzedakis et al., 2017; Yin, 2013) remains debated. A latitudinal shift of the Southern Hemisphere westerlies inducing CO_2 to respire from the Southern Ocean (Kemp et al., 2010) and/or a slowdown of AABW formation (Yin, 2013) have been proposed to be the potential mechanisms for the MBE. In our study, the reduced ventilation observed in this study is consistent with the predicted slowdown in AABW formation after the MBE, corroborating a recent reconstruction of AABW variability in the eastern Pacific (Yi et al., 2023).

5 Conclusions

By studying core MABC−11, this study reveals significant insights into deep-sea ventilation in the Magellan Seamounts during the middle Pleistocene, specifically through the integration of magnetic coercivity, metal enrichment, and sediment grain size. We have determined that the median value of sediment grain size is 3.3 ± 0.2 μm, with minimal changes in clay and silt contents (average values of 52.8 ± 1.8% and 38.2 ± 1.6%, respectively), and greater variability in sand content (average 9.0 ± 2.6%). The dominant magnetic mineral identified is low-coercivity PSD magnetite, with three distinct coercivity subgroups: 6.1 ± 0.5 mT, 25.7 ± 1.0 mT, and 65.2 ± 2.1 mT. By comparing these proxies with various environmental indicators, we proposed that magnetic coercivity and metal enrichment effectively track the signals of deep-sea circulation intensity, whereas sedimentary grain-size changes are more closely linked to eolian inputs with topography-induced influences on the upper ocean. Furthermore, we confirmed that reginal ventilation weakened since the MBE (~430 ka), which likely reflects the reduced AABW formation. This ventilation decrease aligns with previous reconstructions of AABW in the eastern Pacific, and the observed changes in sedimentary dynamics, magnetic minerals, and geochemical proxies provide valuable insights into the broader implications of the MBE on global deep-sea circulation patterns.

Data availability statement

The datasets presented in this study can be found in online repositories. The names of the repository/repositories and accession number(s) can be found in the article/supplementary material.

Author contributions

ZS: Methodology, Project administration, Funding acquisition, Formal Analysis, Writing – review & editing, Writing – original draft. YC: Funding acquisition, Writing – review & editing, Software, Formal Analysis. PM: Software, Writing – review & editing, Formal Analysis. YC: Writing – review & editing, Formal Analysis, Data curation. HW: Data curation, Writing – review & editing, Supervision, Resources, Investigation. LY: Writing – review & editing, Methodology, Funding acquisition, Conceptualization.

Funding

The author(s) declare that financial support was received for the research, authorship, and/or publication of this article. The work was supported by the National Natural Science Foundation of China (42177422, 41602349, 42304084), the China Postdoctoral Science Foundation (2023M743469), and a state assignment of the Far East Geological Institute, Far East Branch, Russian Academy of Sciences (FEGI FEB RAS).

Conflict of interest

The authors declare that the research was conducted in the absence of any commercial or financial relationships that could be construed as a potential conflict of interest.

Publisher's note

References

Ashley, G. M. (1978). Interpretation of polymodal sediments. *J. Geol.* 86, 411–421. doi: 10.1086/649710

Bograd, S. J., Rabinovich, A. B., LeBlond, P. H., and Shore, J. A. (1997). Observations of seamount-attached eddies in the North Pacific. *J. Geophys. Res. Oceans* 102, 12441–12456. doi: 10.1029/97JC00585

Boulay, S., Colin, C., Trentesaux, A., Pluquet, F., Bertaux, J., and Blamart., D. (2003). Mineralogy and sedimentology of Pleistocene sediment in the South China Sea (ODP Site 1144). *Proc. ODP Sci. Results*, 184, 1-21. doi: 10.2973/odp.proc.sr.184.211.2003

Chang, L., Bolton, C. T., Dekkers, M. J., Hayashida, A., Heslop, D., Krijgsman, W., et al. (2016). Asian monsoon modulation of nonsteady state diagenesis in hemipelagic marine sediments offshore of Japan. *Geochem. Geophy. Geosy.* 17, 4383–4398. doi: 10.1002/2016GC006344

Chen, Y., Li, Y., Lyu, W., Xu, D., Han, X., Fu, T., et al. (2020). A 5000-year sedimentary record of East Asian winter monsoon from the northern muddy area of the east China sea. *Atmosphere* 11, 1376. doi: 10.3390/atmos11121376

Chen, Y., Lyu, W., Fu, T., Li, Y., and Yi., L. (2021). Centennial impacts of the east asian summer monsoon on holocene deltaic evolution of the huanghe river, China. *Appl. Sci.* 11, 2799. doi: 10.3390/app11062799

Chen, G., Wang, D., Dong, C., Zu, T., Xue, H., Shu, Y., et al. (2015). Observed deep energetic eddies by seamount wake. *Sci. Rep.* 5, 17416. doi: 10.1038/srep17416

Chen, Y., Xu, D., Qin, H., Liu, G., Li, Y., Chen, W., et al. (2023). Relationships between abyssal redox conditions and rock magnetic properties of surficial sediments in the western pacific. *J. Mar. Sci. Eng.* 11, (6). doi: 10.3390/jmse11061132

Costa, K. M., Anderson, R. F., McManus, J. F., Winckler, G., Middleton, J. L., and Langmuir, C. H. (2018). Trace element (Mn, Zn, Ni, V) and authigenic uranium (aU) geochemistry reveal sedimentary redox history on the Juan de Fuca Ridge, North Pacific Ocean. *Geochim. Cosmochim. Ac.* 236, 79–98. doi: 10.1016/j.gca.2018.02.016

Day, R., Fuller, M., and Schmidt., V. A. (1977). Hysteresis properties of titanomagnetites: Grain-size and compositional dependence. *Phys. Earth Planet. In.* 13, 260–267. doi: 10.1016/0031-9201(77)90108-X

Fedorov, A. V., Burls, N. J., Lawrence, K. T., and Peterson, L. C. (2015). Tightly linked zonal and meridional sea surface temperature gradients over the past five million years. *Nat. Geosci.* 8, 975–980. doi: 10.1038/ngeo2577

Ge, K., Williams, W., Liu, Q., and Yu., Y. (2014). Effects of the core-shell structure on the magnetic properties of partially oxidized magnetite grains: Experimental and micromagnetic investigations. *Geochem. Geophy. Geosy.* 15, 2021–2038. doi: 10.1002/2014GC005265

Gordon, A. L. (2001). "Bottom water formation," in *Encyclopedia of Ocean Sciences, 2nd ed*. Ed. J. H. Steele (Academic Press, Oxford), 415–421. doi: 10.1016/B978-012374473-9.00006-0

Guo, B., Wang, W., Shu, Y., He, G., Zhang, D., Deng, X., et al. (2020). Observed deep anticyclonic cap over caiwei guyot. *J. Geophys. Res. Oceans* 125, e2020JC016254. doi: 10.1029/2020JC016254

Hall, I. R., McCave, I. N., Shackleton, N. J., Weedon, G. P., and Harris, S. E. (2001). Intensified deep Pacific inflow and ventilation in Pleistocene glacial times. *Nature* 412, 809–812. doi: 10.1038/35090552

He, G., Zhao, Z., and Zhu, K. (2001). *Cobalt-Rich Crust Resources in the West Pacific* (Beijing: Geological Publishing House), 1–92.

Heslop, D. (2015). Numerical strategies for magnetic mineral unmixing. *Earth Sci. Rev.* 150, 256–284. doi: 10.1016/j.earscirev.2015.07.007

Heslop, D., and Roberts., A. P. (2012). A method for unmixing magnetic hysteresis loops. *J. Geophys. Res.-Sol. Ea.* 117, B03103. doi: 10.1029/2011JB008859

Hilgen, F. J., Lourens, L. J., Van Dam, J. A., Beu, A. G., Boyes, A. F., Cooper, R. A., et al. (2012). "Chapter 29 - the neogene period," in *The Geologic Time Scale*. Eds. F. M. Gradstein, J. G. Ogg, M. D. Schmitz and G. M. Ogg (Elsevier, Boston), 923–978.

Hodell, D. A., and Venz-Curtis, K. A. (2006). Late Neogene history of deepwater ventilation in the Southern Ocean. *Geochem. Geophy. Geosy.* 7, Q09001. doi: 10.1029/2005gc001211

Hu, B., Yi, L., Zhao, J., Guo, J., Ding, X., Wang, F., et al. (2021). Magnetostratigraphy of core XT06 and Quaternary sedimentary dynamics of the deep-sea deposits in the West Philippine Basin. *Mar. Geol. Quat. Geol.* 41, 61–74. doi: 10.16562/j.cnki.0256-1492.2020101301

Jackson, M., Worm, H.-U., and Banerjee, S. K. (1990). Fourier analysis of digital hysteresis data: rock magnetic applications. *Phys. Earth Planet. In.* 65, 78–87. doi: 10.1016/0031-9201(90)90077-B

Jacobel, A. W., McManus, J. F., Anderson, R. F., and Winckler., G. (2017). Repeated storage of respired carbon in the equatorial Pacific Ocean over the last three glacial cycles. *Nat. Commun.* 8, 1727. doi: 10.1038/s41467-017-01938-x

Jansen, J. H. F., Kuijpers, A., and Troelstra., S. R. (1986). A mid-brunhes climatic event: long-term changes in global atmosphere and ocean circulation. *Science* 232, 619–622. doi: 10.1126/science.232.4750.619

Jiang, Z., Sun, Z., Liu, Z., Cao, H., Geng, W., Xu, H., et al. (2019). Rare-earth element geochemistry reveals the provenance of sediments on the southwestern margin of the Challenger Deep. *J. Oceanol. Limnol.* 37, 998–1009. doi: 10.1007/s00343-019-8046-8

Johnson, G. C. (2008). Quantifying antarctic bottom water and north atlantic deep water volumes. *J. Geophysical Research: Oceans* 113, C05027. doi: 10.1029/2007jc004477

Kawabe, M., and Fujio, S. (2010). Pacific ocean circulation based on observation. *J. Oceanogr.* 66, 389–403. doi: 10.1007/s10872-010-0034-8

Kemp, A. E. S., Grigorov, I., Pearce, R. B., and Naveira Garabato, A. C. (2010). Migration of the Antarctic Polar Front through the mid-Pleistocene transition: evidence and climatic implications. *Quaternary Sci. Rev.* 29, 1993–2009. doi: 10.1016/j.quascirev.2010.04.027

Kissel, C., Laj, C., Jian, Z., Wang, P., Wandres, C., and Rebolledo-Vieyra., M. (2020). Past environmental and circulation changes in the South China Sea: Input from the magnetic properties of deep-sea sediments. *Quat. Sci. Rev.* 236, 106263. doi: 10.1016/j.quascirev.2020.106263

Kruiver, P. P., and Passier, H. F. (2001). Coercivity analysis of magnetic phases in sapropel S1 related to variations in redox conditions, including an investigation of the S ratio. *Geochem. Geophy. Geosy.* 2, (12). doi: 10.1029/2001GC000181

Lamy, F., Winckler, G., Arz, H. W., Farmer, J. R., Gottschalk, J., Lembke-Jene, L., et al. (2024). Five million years of Antarctic Circumpolar Current strength variability. *Nature* 627, 789–796. doi: 10.1038/s41586-024-07143-3

Lavelle, J. W., and Mohn, C. (2010). Motion, commotion, and biophysical connections at deep ocean seamounts. *Oceanography* 23, 90–103. doi: 10.5670/oceanog.2010.64

Li, J., Liu, Y., Liu, S., Roberts, A. P., Pan, H., Xiao, T., et al. (2020). Classification of a complexly mixed magnetic mineral assemblage in pacific ocean surface sediment by electron microscopy and supervised magnetic unmixing. *Front. Earth Sci.* 8. doi: 10.3389/feart.2020.609058

Lin, Z., Yi, L., Wang, H., Deng, X., Yang, J., Fu, T., et al. (2019). Rock magnetism of deep-sea sediments at Caiwei Guyot, Magellan seamounts of Northwest Pacific and its significance to abyssal environmental changes. *Chin. J. Geophys.* 62, 3067–3077. doi: 10.6038/cjg2019M0526

Lisiecki, L. E., and Raymo, M. E. (2005). A Pliocene-Pleistocene stack of 57 globally distributed benthic $\delta^{18}O$ records. *Paleoceanography* 20, PA1003. doi: 10.1029/2004pa001071

Liu, Q., Huo, Y.-Y., Wu, Y.-H., Bai, Y., Yuan, Y., Chen, M., et al. (2019). Bacterial community on a guyot in the northwest pacific ocean influenced by physical dynamics and environmental variables. *J. Geophys. Res.-Biogeo.* 124, 2883–2897. doi: 10.1029/2019JG005066

Liu, W., Liu, Z., Sun, J., Song, C., Chang, H., Wang, H., et al. (2020). Onset of permanent Taklimakan Desert linked to the mid-Pleistocene transition. *Geology* 48, 782–786. doi: 10.1130/G47406.1

Löwemark, L., März, C., O'Regan, M., and Gyllencreutz., R. (2014). Arctic Ocean Mn-stratigraphy: genesis, synthesis and inter-basin correlation. *Quat. Sci. Rev.* 92, 97–111. doi: 10.1016/j.quascirev.2013.11.018

Maxbauer, D. P., Feinberg, J. M., and Fox, D. L. (2016). MAX UnMix: A web application for unmixing magnetic coercivity distributions. *Comput. Geosci-UK* 95, 140–145. doi: 10.1016/j.cageo.2016.07.009

Özdemir, Ö, and Dunlop, D. J. (2010). Hallmarks of maghemitization in low-temperature remanence cycling of partially oxidized magnetite nanoparticles. *Geophys. Res.-Sol. Ea* 115, B02101. doi: 10.1029/2009JB006756

Paillard, D. (1998). The timing of Pleistocene glaciations from a simple multiple-state climate model. *Nature* 391, 378–381. doi: 10.1038/34891

Paterson, G. A., and Heslop, D. (2015). New methods for unmixing sediment grain size data. *Geochem. Geophy. Geosy.* 16, 4494–4506. doi: 10.1002/2015gc006070

Perfect, B., Kumar, N., and Riley., J. J. (2018). Vortex structures in the wake of an idealized seamount in rotating, stratified flow. *Geophys. Res. Lett.* 45, 9098–9105. doi: 10.1029/2018GL078703

Rea, D. K. (1994). The paleoclimatic record provided by eolian deposition in the deep sea: The geologic history of wind. *Rev. Geophys.* 32, 159–195. doi: 10.1029/93RG03257

Roberts, A. P., Tauxe, L., Heslop, D., Zhao, X., and Jiang, Z. (2018). A critical appraisal of the "Day" Diagram. *J. Geophys. Res.-Sol. Ea.* 123, 2618–2644. doi: 10.1002/2017JB015247

Robertson, R., Dong, J., and Hartlipp, P. (2017). Diurnal critical latitude and the latitude dependence of internal tides, internal waves, and mixing based on barcoo seamount. *J. Geophys. Res. Oceans* 122, 7838–7866. doi: 10.1002/2016JC012591

Schmidt, H., Berger, W., Bickert, T., and Wefer., G. (1993). "Quaternary carbon isotope record of pelagic foraminifers: Site 806, Ontong Java Plateau," in *Proceedings of the Ocean Drilling Program, Scientific Results*. Eds. W. Berger, L. Kroenke, T. Janecek, J. Backman, F. Bassinot and R. Corfield (Ocean Drilling Program, College Station, TX, USA), 397–409.

Slemons, L., Paul, B., Resing, J., and Murray, J. W. (2012). Particulate iron, aluminum, and manganese in the Pacific equatorial undercurrent and low latitude western boundary current sources. *Mar. Chem.* 142-144, 54–67. doi: 10.1016/j.marchem.2012.08.003

Stepashko, A. A. (2008). Spreading cycles in the pacific ocean. *Oceanology* 48, 401–408. doi: 10.1134/S0001437008030120

Sun, Y., Gao, S., and Li, J. (2003). Preliminary analysis of grain-size populations with environmentally sensitive terrigenous components in marginal sea setting. *Chin. Sci. Bull.* 48, 184–187. doi: 10.1360/03tb9038

Sun, Q., Song, J., Li, X., Yuan, H., Ma, J., and Wang, Q. (2020). Bacterial vertical and horizontal variability around a deep seamount in the Tropical Western Pacific Ocean. *Mar. pollut. Bull.* 158, 111419. doi: 10.1016/j.marpolbul.2020.111419

Talley, L. D. (2008). Freshwater transport estimates and the global overturning circulation: Shallow, deep and throughflow components. *Prog. Oceanogr.* 78, 257–303. doi: 10.1016/j.pocean.2008.05.001

Tzedakis, P. C., Crucifix, M., Mitsui, T., and Wolff., E. W. (2017). A simple rule to determine which insolation cycles lead to interglacials. *Nature* 542, 427–432. doi: 10.1038/nature21364

Wang, F., He, G., Wang, H., and Ren, J. (2016a). Geochemistry of rare Earth elements in a core from Mariana Trench and its significance. *Mar. Geol. Quat. Geol.* 36, 67–75. doi: 10.16562/j.cnki.0256-1492.2016.04.008

Wang, X., Li, H., Zhang, J., Chen, J., Xie, X., Xie, W., et al. (2024). Seamounts generate efficient active transport loops to nourish the twilight ecosystem. *Sci. Adv.* 10, eadk6833. doi: 10.1126/sciadv.adk6833

Wang, Y., Zhang, H., Liu, J., Zhang, X., and Zhu, B. (2016b). Abundances and spatial distributions of associated useful elements in Corich crusts from Caiwei Seamount in Magellan Seamounts. *Mar. Geol. Quat. Geol.* 36, 65–74. doi: 10.16562/j.cnki.0256-1492.2016.02.008

Wei, Z., Deng, X., Zhu, K., Yao, H., Yang, Y., and Ren, J. (2017). Characteristic of substrate rocks of Caiwei Seamounts in the west Pacific Ocean. *Mar. Geol. Front.* 33, 1–6. doi: 10.16028/j.1009-2722.2017.12001

Wessel, P. (1997). Sizes and ages of seamounts using remote sensing: implications for intraplate volcanism. *Science* 277, 802–805. doi: 10.1126/science.277.5327.802

Wessel, P., and Lyons, S. (1997). Distribution of large Pacific seamounts from Geosat/ERS-1: Implications for the history of intraplate volcanism. *J. Geophys. Res.-Sol. Ea.* 102, 22459–22475. doi: 10.1029/97JB01588

Xu, Z., Li, T., Clift, P. D., Lim, F., Wan, S., Chen, H., et al. (2015). Quantitative estimates of Asian dust input to the western Philippine Sea in the mid-late Quaternary and its potential significance for paleoenvironment. *Geochem. Geophy. Geosy.* 16, 3182–3196. doi: 10.1002/2015GC005929

Xu, P., Liu, F., Ding, Z., and Wang, C. (2016). A new species of the thorid genus Paralebbeus Bruce & Chace 1986 (Crustacea: Decapoda: Caridea) from the deep sea of the Northwestern Pacific Ocean. *Zootaxa* 4085, 119–126. doi: 10.11646/zootaxa.4085.1.5

Yamazaki, T. (2012). Paleoposition of the Intertropical Convergence Zone in the eastern Pacific inferred from glacial-interglacial changes in terrigenous and biogenic magnetic mineral fractions. *Geology* 40, 151–154. doi: 10.1130/g32646.1

Yang, Z., Qian, Q., Chen, M., Zhang, R., Yang, W., Zheng, M., et al. (2020). Enhanced but highly variable bioturbation around seamounts in the northwest Pacific. *Deep-Sea Res. Part I* 156, 103190. doi: 10.1016/j.dsr.2019.103190

Yang, S., Xing, J., Chen, D., and Chen, S. (2017). A modelling study of eddy-splitting by an island/seamount. *Ocean Sci.* 13, 837–849. doi: 10.5194/os-13-837-2017

Yao, H., Wang, F., Wang, H., Yu, M., Ren, J.-b., He, G., et al. (2021). Pleistocene magnetostratigraphy of four cores in the West Philippian Basin and regional sedimentary shift during the Mid-Pleistocene transition. *Geol. J.* 56, 2919–2929. doi: 10.1002/gj.4082

Yi, L. (2023). Diverse glacial ventilation in deep Pacific: An integrated record from Mariana Trench and Magellan Seamounts over last 1.2 Myr. *Global Planet. Change* 230, 104279. doi: 10.1016/j.gloplacha.2023.104279

Yi, L., Hu, B., Zhao, J., Jiang, X., Shu, Y., Wang, X., et al. (2022). Magnetostratigraphy of abyssal deposits in the central philippine sea and regional sedimentary dynamics during the quaternary. *Paleoceanogr. Paleocl.* 37, e2021PA004365. doi: 10.1029/2021PA004365

Yi, L., Li, Y., Mikhailik, P., Qi, Y., and Deng, C. (2023). Magnetic and geochemical scanning reveals growth history of marine ferromanganese crust on Detroit Seamount, northwest Pacific since the early Miocene. *Quat. Int.* 671, 52–61. doi: 10.1016/j.quaint.2023.08.002

Yi, L., Wang, H., Deng, X., Yuan, H., Xu, D., and Yao, H. (2021a). Geochronology and geochemical properties of mid-pleistocene sediments on the caiwei guyot in the northwest pacific imply a surface-to-deep linkage. *J. Mar. Sci. Eng.* 9, (3). doi: 10.3390/jmse9030253

Yi, L., Wang, H., Liu, G., Chen, Y., Yao, H., and Deng, X. (2021b). Magnetic minerals in Mid-Pleistocene sediments on the Caiwei Guyot, Northwest Pacific and their response to the Mid-Brunhes climate event. *Acta Oceanol. Sini.* 40, 1–11. doi: 10.1007/s13131-021-1872-5

Yi, L., Xu, D., Jiang, X., Ma, X., Ge, Q., Deng, X., et al. (2020). Magnetostratigraphy and authigenic $^{10}Be/^{9}Be$ dating of plio-pleistocene abyssal surficial sediments on the southern slope of mariana trench and sedimentary processes during the mid-pleistocene transition. *J. Geophys. Res. Oceans* 125, e2020JC016250. doi: 10.1029/2020JC016250

Yi, L., Yu, H.-J., Ortiz, J. D., Xu, X.-Y., Chen, S.-L., Ge, J.-Y., et al. (2012a). Late Quaternary linkage of sedimentary records to three astronomical rhythms and the Asian monsoon, inferred from a coastal borehole in the south Bohai Sea, China. *Palaeogeogr. Palaeoclimatol. Palaeoecol.* 329-330, 101–117. doi: 10.1016/j.palaeo.2012.02.020

Yi, L., Yu, H., Ortiz, J. D., Xu, X., Qiang, X., Huang, H., et al. (2012b). A reconstruction of late Pleistocene relative sea level in the south Bohai Sea, China, based on sediment grain-size analysis. *Sediment. Geol.* 281, 88–100. doi: 10.1016/j.sedgeo.2012.08.007

Yin, Q. (2013). Insolation-induced mid-Brunhes transition in Southern Ocean ventilation and deep-ocean temperature. *Nature* 494, 222–225. doi: 10.1038/nature11790

Zhai, F., and Gu, Y. (2020). Abyssal circulation in the Philippine sea. *J. Ocean U. China* 19, 249–262. doi: 10.1007/s11802-020-4241-7

Zhang, X., and Boyer, D. L. (1991). Current deflections in the vicinity of multiple seamounts. *J. Phys. Oceanogr.* 21, 1122–1138. doi: 10.1175/1520-0485(1991)021<1122:CDITVO>2.0.CO;2

Zhang, X., and Boyer, D. L. (1993). Laboratory study of rotating, stratified, oscillatory flow over a seamount. *J. Phys. Oceanogr.* 23, 1122–1141. doi: 10.1175/1520-0485(1993)023<1122:LSORSO>2.0.CO;2

Zhang, W., De Vleeschouwer, D., Shen, J., Zhang, Z., and Zeng, L. (2018). Orbital time scale records of Asian eolian dust from the Sea of Japan since the early Pliocene. *Quat. Sci. Rev.* 187, 157–167. doi: 10.1016/j.quascirev.2018.03.004

Zhao, B., Wei, Z., Yang, Y., He, G., Zhang, H., and Ma, W. (2020). Sedimentary characteristics and the implications of cobalt-rich crusts resources at Caiwei Guyot in the Western Pacific Ocean. *Mar. Georesour. Geotec.* 38, 1037–1045. doi: 10.1080/1064119X.2019.1648615